



Contents lists available at ScienceDirect

Journal of King Saud University – Science

journal homepage: www.sciencedirect.com

Original article

Oxovanadium(IV) complex of 8-hydroxy quinoline and 3-acetyl-6-methyl-2H-pyran-2,4(3H)-dione: Experimental, theoretical and antibacterial evaluation

J.M. Mir*, D.K. Rajak, R.C. Maurya

Bioinorganic and Computational Chemistry Laboratory, Department of P. G. Studies and Research in Chemistry and Pharmacy, R. D. University, Jabalpur 482001, MP, India

ARTICLE INFO

Article history:

Received 19 January 2018

Accepted 26 March 2018

Available online 28 March 2018

Keywords:

Oxovanadium

DFT

Spectroscopy

Bactericidal

ABSTRACT

Streptococcus pyogenes and *E. coli* are causative agents of millions of illness. In conspicuous interests to design antibiotic compounds against these bugs, a novel oxovanadium(IV) complex containing dehydroacetic acid (3-acetyl-6-methyl-2H-pyran-2,4(3H)-dione) and 8-hydroxy quinoline was synthesized and characterized. Elemental analyses, thermal degradation, molar conductance, magnetic susceptibility, EPR, mass spectrometry and FT-IR spectral techniques were used to formulate the compound. Theoretical aspects like geometrical optimization, molecular charge density plots and DFT based spectroscopy were also invoked using Gaussian 09 software package by the help of Becke-3-Lee-Yang-Parr (B3LYP) hybrid exchange-correlation functional and the standard basis set LANL2DZ. At each step of characterization, theoretical and experimental results were compared to arrive at the best fit results. From the different spectral analyses a suitable octahedral structure can be proposed for the complex. In addition to formulation, the complex and dhaH were biologically tested against some bacterial strains. The target complex was found less bactericidal against *E. coli*, but the results have shown satisfactory bacterial activity against *S. pyogenes*.

© 2018 The Authors. Production and hosting by Elsevier B.V. on behalf of King Saud University. This is an open access article under the CC BY-NC-ND license (<http://creativecommons.org/licenses/by-nc-nd/4.0/>).

1. Introduction

Vanadium complexes generally exist in IV and V oxidation states (Singh et al., 2013). The complexes are well known for possessing excellent biological activity (Mir et al., 2017a,b). During the design of these complexes, compounds falling in the range of small molecular weights are preferably given attention (Sasmal et al., 2008). Novel anti-diabetic medicines/drugs are designed from vanadium (Liu et al., 2014). Under such curiosity, treatment for both the general types of diabetes in various animal models is under trials (Thompson and Orvig, 2006). Two well known complexes, despite some toxicity, bis(maltolato)Oxovanadium(IV) (BMOV) and bis(ethylmaltolato)Oxovanadium(IV) (BEOV) have been proven for hyperglycemic action (Maurya et al., 2014). Hence,

great efforts are in practice to develop potent biological relevant molecules of this suit. So, many oxovanadium(IV) complexes having varied coordination modes have been thus prepared and put forth for the respective examination (Malik and Mir, 2018; Früh et al., 2014).

In order to synthesize an applicable novel metallic complex, it has always been a meticulous job to select the multifold significant organic-framework. In the present case, dehydroacetic acid and 8-hydroxy quinoline represent compounds of diverse importance. The pyrone derivative, dhaH is used for preparation of a large number of heterocyclic compounds bearing well pronounced anti-microbial properties (Jilalat et al., 2017). The use of this compound as a food preservative justifies its human-friendly nature (Vishwakarma et al., 2016). On the other side, quinoline derivatives are also potent therapeutic compounds (Kumar et al., 2009). Their anti-protozoal, antiseptic and antiperspirant properties are enough to attract researchers. Therefore, much interest has been directed towards synthesis and characterization of complexes of such type of ligands (Mandewal et al., 2016). In the search for more efficacious insulin-mimic complexes, the targeted ligand-complexation can also be proposed to be an addition to the same class of compounds (Maurya et al., 2015).

* Corresponding author.

E-mail address: mirjanmohammad@gmail.com (J.M. Mir).

Peer review under responsibility of King Saud University



Production and hosting by Elsevier

In the present era, molecular characterization is validated by theoretical evaluation of a problem. Density functional theory (DFT) is considered as a strong theoretical front to complement with experimental formulation. Almost every spectral technique can be justified by taking a tally with DFT results. Hence it results in a wide use of computational methods. The technique is considered as a substitute to X-ray crystallography for the complexes where crystal-growth fails. Many studies are evident that it is a powerful method for predicting and solving geometrical problems of a known or unknown compound (Micera and Garribba, 2011a,b; Garribba et al., 2011; Rodrigues, 2011).

In prominent evidences in support of the importance of vanadium complexes and the utility of computational DFT studies, a systematic approach to prepare and characterize mixed ligand complex of oxovanadium(IV) containing 3-acetyl-6-methyl-2H-pyran-2,4(3H)-dione (dhaH) and 8-hydroxy quinoline (8-hqH) as ligands was aimed. The respective biological, thermal and DFT investigations are the main parts of the study.

2. Experimental

2.1. Materials and methods

Vanadium sulphate pentahydrate (Aldrich chemical Co. USA), 3-acetyl-6-methyl-2H-pyran-2,4(3H)-dione (dhaH) (Merck Specialties Pvt., Ltd. Bombay), 8-Hydroxy quinoline, (Merck) 2-picolinic acid and DMF (Thomas Baker (Chemical) Ltd. Mumbai), ethanol (Bengal Chemical and Pharmaceuticals Ltd.) were used as received. All the chemicals were of analytical reagent grade.

2.2. Analysis

Elemental composition (CHN) was determined micro-analytically at S.A.I.F., I.I.T. Powai, Mumbai. The vanadium content was determined by following a slightly modified procedure reported elsewhere (Maurya et al., 2015). 50 mg weight of the sample placed in a silica crucible was decomposed by mixing in 2–3 mL of concentrated HNO₃ and heating. An orange colored solid (V₂O₅) which was obtained was allowed to get completely dissolved in a minimum amount of dilute H₂SO₄, and the resulting solution was diluted to 100 mL by adding distilled water. Volumetric estimation of vanadium was finally done using 0.02 M KMnO₄ solution as an oxidizing agent in the presence of sulfurous acid (H₂SO₃).

THERMO Finnigan LCQ Advantage max ion trap mass spectrometer, Bruker alpha-T model FT-IR spectrophotometer and Varian Cary 5000 double beam UV-Vis spectrophotometer were used to record mass, IR and electronic spectra, respectively. Cyclic voltammetry was carried out using tetra butyl ammonium perchlorate (TBAP) as a supporting electrolyte on epsilon BASI. Magnetic, conductance and decomposition records were made on SHERWOOD Scientific UK, Toshniwal Conductivity Bridge and melting point apparatus (Kumar Industries, Mumbai), respectively. Thermogravimetric analysis and EPR spectrum were recorded at SAIF, IIT Mumbai.

Theoretical aspects of the complex was studied using density functional theory (DFT) level under B3LYP/6-311+G specified for nonmetallic atoms and B3LYP/LANL2DZ for vanadium atom. The Gauss View 5.0, a graphical interface associated with Gaussian program was carefully visualized to identify the related vibrational modes for the respective IR calculations (GaussView 5.0). After obtaining zero imaginary frequency in the respective FT-IR simulation it is ascertained that the optimized geometry is a local minima. In addition to frequency calculations, various charge density plots confined to different theories were also evaluated to deepen

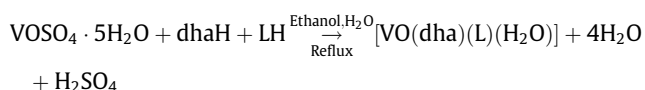
the theoretical speculation of chemical descriptors. The energies of the various molecular orbitals, especially highest occupied molecular orbital (HOMO) and lowest unoccupied molecular orbital (LUMO) levels along with the determination of intramolecular charge transfer (ICT) represents the theoretical route adopted in the investigation (Frisch et al., 2010).

2.3. Preparation of mixed-ligand complex

0.001 M dehydroacetic acid (0.168 g) dissolved in 10 mL of ethanol was mixed with 10 mL ethanolic solution of 0.001 M 8-hydroxy quinoline, (0.145 g). The resulting binary solution was slowly added to the solution of 0.001 M VOSO₄·5H₂O (0.253 g) in 10 mL of ethanol-water (1:1) under constant stirring at 50 °C. A coloured solid began to start precipitating slowly after the ternary mixture was allowed to reflux for 2–3 h, which was finally suction filtered, repeatedly washed with 1:1 ethanol-water and dried in vacuo.

3. Results and discussions

The mixed-ligand oxovanadium(IV) complex in the present was synthesized by the process shown below:



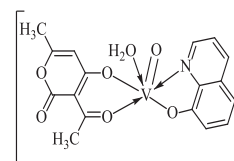
Where, dhaH = dehydroacetic acid, LH = 8-hydroxyquinolene. The complex was found to be air stable solid substance and the respective solubility tests in various solvents showed that the compound was unable to get dissolved in most of the common organic solvents but showed solubility in DMF, DMSO, and acetonitrile.

Analytical data: Empirical formula: C₁₅H₁₇NO₇V, Molecular weight: 396, Color: Venetian Green, Yield(%): 65, Melting Point (°C): 300, μ_{eff} (B.M.): 1.72, Molar conductance ($\Omega^{-1} \text{cm}^2 \cdot \text{mol}^{-1}$): 19.7, Elemental analysis Calculated(Observed)%: C 51.53 (56.30), H 3.82 (3.75), N 3.53 (3.58), V 12.86 (12.80)

The proposed structure of the complex is shown in Scheme 1.

3.1. Infrared spectral studies

The FTIR analysis of the complex shows that the complex exhibits a strong band in the range 640–655 cm⁻¹, which can be assigned to V=O. The $\nu(\text{V}=\text{O})$ is found at 974–975 cm⁻¹ suggesting the absence of V=O...V=O unit (Maurya et al., 2001). The broad band located at 3418 cm⁻¹ in the IR spectrum of dhaH ligand which is due to hydrogen bonded $\nu(\text{OH})$, and a medium band centered at 1236 cm⁻¹ representing $\nu(\text{C}=\text{O})$ (enolic) suggests the enolic form in solid state. The band due to the $\nu(\text{OH})$ of the ligands disappears in the respective complex after deprotonation. The appearance of strong band in the range 1644–1662 cm⁻¹ may be assigned to $\nu(\text{C}=\text{N})$ (Mir et al., 2016). Moreover, the appearance of a strong band at ~1106 cm⁻¹ in the complex suggests the coordination of the hydroxyl oxygen of the ligand. These results support the bidentate coordination of 8-hydroxyquinolene. The complex also shows a broad band vibrational peak at 3441 cm⁻¹



Scheme 1. 2D-Structure of Complex.

assignable to $\nu(\text{OH})$ mode due to the coordinated H_2O (Maurya et al., 2015). The respective IR spectrum is given in Fig. 1. Fig. 2 is the theoretical FTIR spectrum of the complex. On comparing the results discussed in the experimental section of this sort, it can be established that the DFT-based infra-red spectral data is in excellent agreement with the results being reported.

3.2. Magnetic measurements and conductance measurements

The observed value of the magnetic moment of the complex is 1.72B.M., as expected for magnetically dilute oxovanadium(IV) complexes. Similarly, experimentally determined molar conductance measured in 10^{-3} M dimethylformamide (DMF) solution of the complex gestures the non-electrolytic behaviour (Popova et al., 2015).

3.3. Mass spectrometry

The electron spray ionization (ESI) (Fig. S1) mass spectral analysis was carried out to confirm the molecular formula of the complex. The representative compound $[\text{VO}(\text{dha})(8\text{-hq})(\text{H}_2\text{O})]$ gives

spectral peaks at 396, 168, 144 m/z indicating [molecular ion]⁺, (396), $[\text{dha} + \text{H}]^+ = 169$ and $[\text{8hq} + \text{H}]^+ = 144$. The m/z 195 can be because of oxovanadium binded cation with quinoline moiety (devoid of hydroxyl oxygen). The results are in good agreement with the proposed molecular composition of the complex.

3.4. Electronic spectral studies

Fig. 3 shows the electronic spectral record of the representative complex $[\text{VO}(8\text{-hq})(\text{dha})\text{H}_2\text{O}]$ carried out in 10^{-3} M DMSO solution. The high intensity peak(s) in the region 263 nm are attributed to intra ligand $n \rightarrow \pi^*/\pi \rightarrow \pi^*$ type transitions. The lower intensity peak(s) around 402 nm may be assigned to ligand to metal charge transfer (LMCT) transitions (Maurya et al., 2002). The theoretically generated electronic spectrum (Fig. 4) using the TD-DFT method and DMSO as the solvent at B3LYP/LANL2DZ level of theory shows mainly six bands at 473, 482, 489, 613 and 652 nm. The overall analysis shows close agreement only confined to 400 nm region. The reason of poor agreement can be the less reliability of the theory used for the computation.

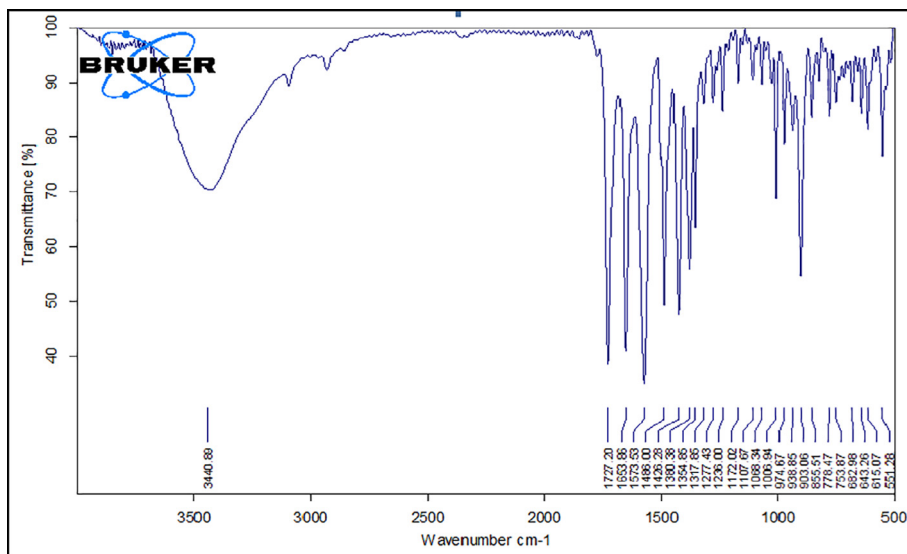


Fig. 1. Experimental FT-IR spectrum of $[\text{VO}(\text{dha})(8\text{-hq})(\text{H}_2\text{O})]$

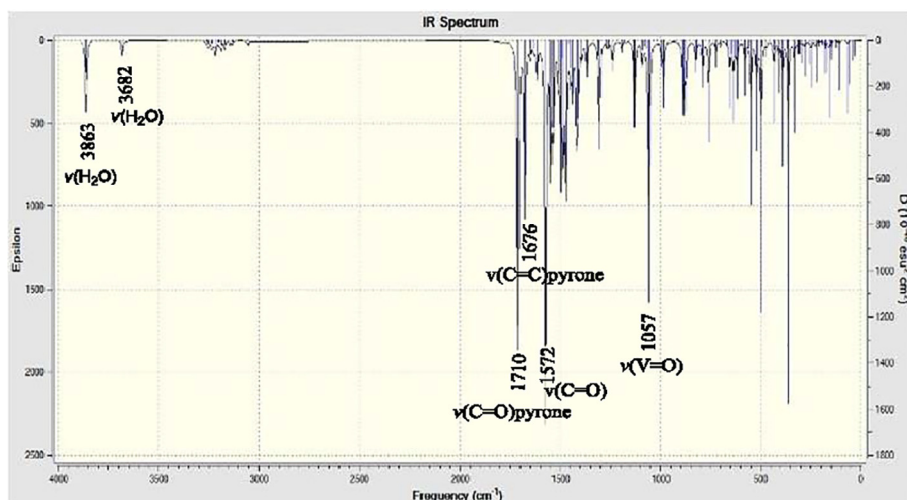


Fig. 2. Theoretical FT-IR spectrum of $[\text{VO}(\text{dha})(8\text{-hq})(\text{H}_2\text{O})]$

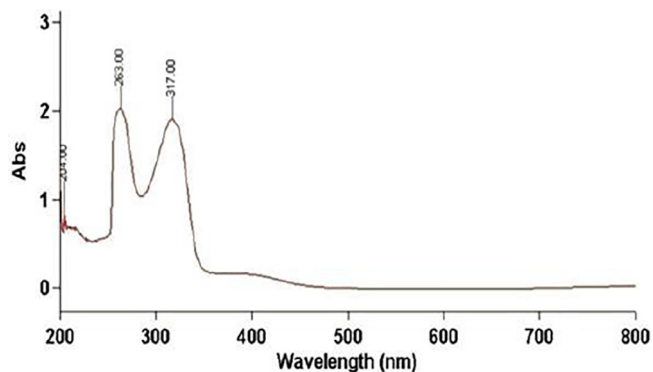


Fig. 3. Experimental electronic spectrum of complex [VO(8-hq)(dha)H₂O]

3.5. Thermogravimetric analysis

Thermogravimetric curve of the compound, [VO(dha)(8-hq)(H₂O)] is given in Fig. S2. The analysis was carried out in the temperature range of 20–1000 °C at the heating rate of 10 °C/min. Despite the fact that the complex did not show a usual decomposition pattern as expected for the complexes under question. But it can be stated that simultaneous mass losses can also happen under thermal analysis. This unexpected behaviour can be correlated with the similar type of results reported elsewhere (Diaz et al., 2015; Valenzuela et al., 2013). The weight loss of 48.77% at 25–370 °C, can be corresponded to the removal of one molecule of coordinated water (Dodd et al., 1987) and one molecule of dehydroacetic acid anion per molecule of the complex (calculated weight loss = 46.71%). The further raise of temperature under the same heating rate shows two more weight losses, whose correla-

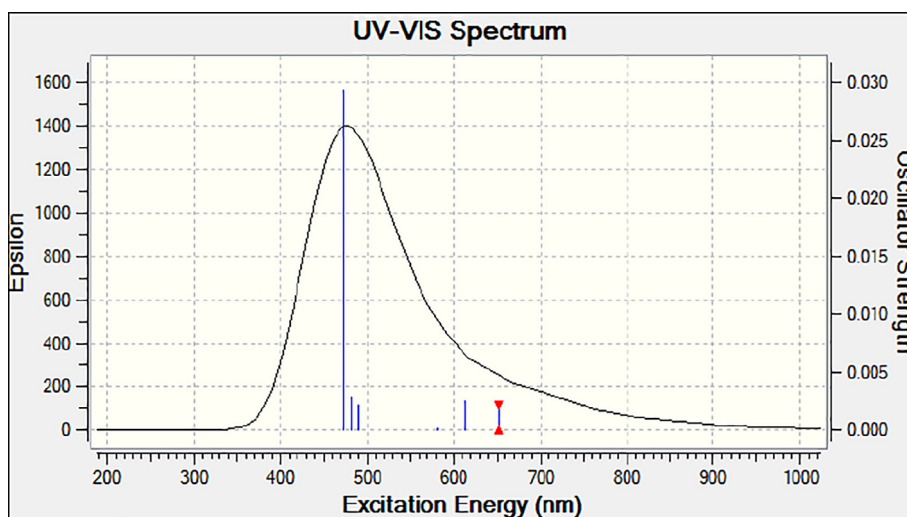


Fig. 4. TD-DFT Theoretical electronic spectrum of complex [VO(8-hq)(dha)H₂O]

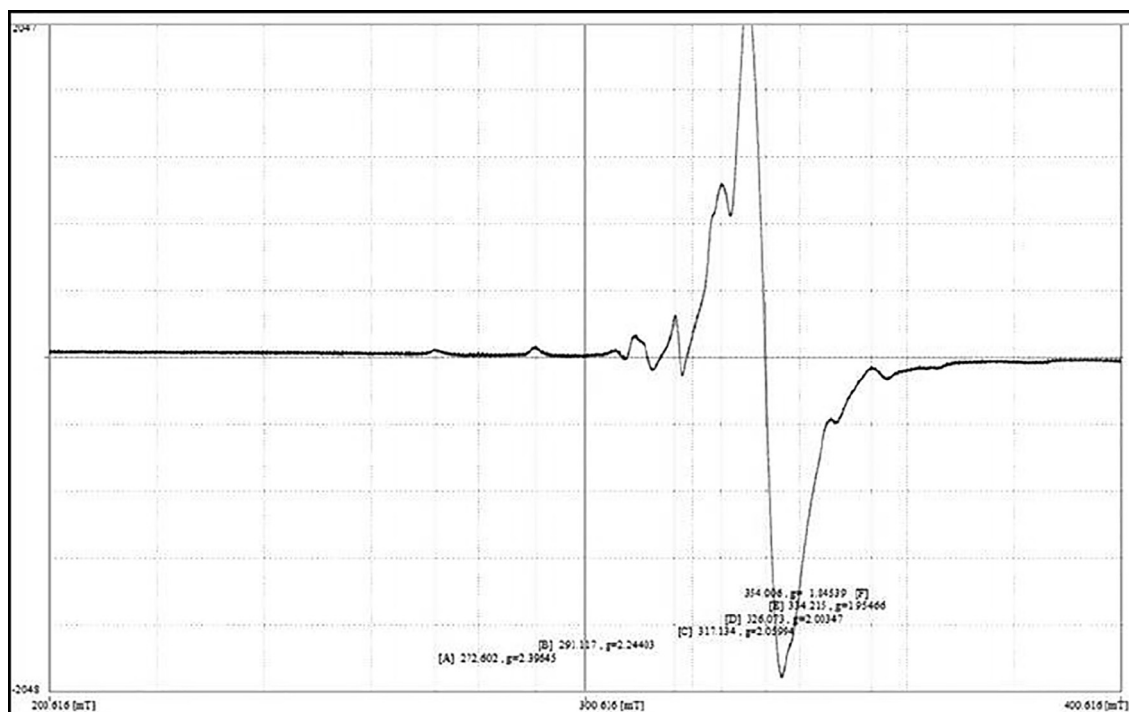


Fig. 5. ESR spectrum of complex [VO(dha)(8-hq)(H₂O)] (1).

tion could not be made separately. However, the mass degradation in the temperature range 370–820 °C (observed 22.51%) (calcd. 27.7%, can be considered the loss for 1 mol of 8-hq ligand roughly estimated to the removal of one coordinated group. The final residue confined to an invariable weight (observed 28.88%) over 820 °C roughly corresponds to V_2O_5 (calcd. 25.59%).

3.6. Electron paramagnetic resonance studies

From the EPR Spectrum of the complex shown in Fig. 5, the confirmation of unpaired electron in the vicinity of $I = 7/2$ of its own mother nucleus gives $(2 \times 7/2 + 1)$ 8 line spectrum. The observed spectral parameters for this compound are: g_{\perp} 2.030, g_{\parallel} 2.0806, $g_{av} = 2.046$. The observed g_{av} value deviates from the free ion value 2.0036, indicates that the complex is appreciably covalent. The respective data has been tabulated in Table 5. The g_{\parallel} and g_{\perp} values in the complex ensues the respective covalent nature (Dutta and Syamal, 1993). The features of spectrum indicates monomeric oxovanadium(IV) complex (Maurya et al., 2002).

3.7. Electrochemical properties

To understand the spectral and structural changes that occur on redox activity of the complex, cyclic voltammetry was invoked. The analysis was carried out in the DMSO vs Ag/AgCl reference electrode at scan rate of 100 mVs^{-1} under the potential range of -1500 to $+1500$ mV in the co-existence of 0.1 M of tetrabutylammonium perchlorate (TBAP) as a supporting electrolyte. The results have shown that the vanadyl complex exhibits one electron quasi-reversible transfer process with a reduction peak at $E_{pc} = -447$ to -471 and corresponding oxidation peak at $E_{pa} = -295$ to -322 (Fig. S3). Overall the complex shows a predominant reduction. The respective redox couples with peak gap values (ΔE_p) ranging from 125 to 175 mV, clarifies the presence of a single step one electron transfer process. The negative E_r potentials (-383 to -384 mV) may be assigned to the corresponding V(IV) to V(III) conversion (Dai et al., 1996; Maurya and Rajput, 2004). ΔE_p value can be seen showing an increasing trend with the increasing in scan rates, supporting the evidence for the quasi-reversible V(IV)/V(III) couple.

4. Computational studies

4.1. Geometrical parameters

Geometry optimization is the first and foremost computational process that is generally established to get insights regarding atomic projections to attain energy minimal state of the complex. The z-matrix presentation of different geometry elements of the optimized structure of the complex, $[\text{VO}(\text{dha})(8\text{-hq})(\text{H}_2\text{O})]$ are given in the Table 1. The optimized structure of the compound (1) is shown in Fig. 6. The computed bond lengths, such as, $\text{V}=\text{O}$ (oxo) (14), $\text{V}-\text{O}$ (enolic) (11), $\text{V}-\text{O}$ (ketonic) (1), $\text{V}-\text{O}$ (water) (26), $\text{V}-\text{O}$ (25) and $\text{V}-\text{N}$ (15), in the present complex are 1.6074, 2.1703, 1.9939, 2.1528, 1.9261 and 2.1108 Å, respectively. These results are comparable to the data reported elsewhere (Greenwood and Earnshaw, 1984). $\text{O}(1)-\text{V}(13)-\text{O}(11)$, (75.0591°), $\text{O}(1)-\text{V}(13)-\text{O}(14)$, (100.9314°), $\text{O}(1)-\text{V}(13)-\text{O}(25)$, (88.3392°), $\text{O}(1)-\text{V}(13)-\text{O}(26)$, (93.4652°), $\text{O}(11)-\text{V}(13)-\text{N}(15)$, (84.5678°), $\text{O}(11)-\text{V}(13)-\text{O}(25)$, (90.2716°), $\text{O}(11)-\text{V}(13)-\text{O}(26)$, (72.0918°), $\text{O}(14)-\text{V}(13)-\text{N}(15)$, (98.2726°), $\text{O}(14)-\text{V}(13)-\text{O}(25)$, (110.0045°), $\text{O}(14)-\text{V}(13)-\text{O}(26)$, (87.7144°), $\text{O}(25)-\text{V}(13)-\text{N}(15)$, (80.6722°), $\text{N}(15)-\text{V}(13)-\text{O}(26)$, (91.9625°), $\text{O}(14)-\text{V}(13)-\text{O}(11)$, (159.724°), $\text{O}(25)-\text{V}(13)-\text{O}(26)$, (161.535°), $\text{O}(1)-\text{V}(13)-\text{N}(15)$, (160.225°). From

Table 1
Geometrical parameters of optimized complex $[\text{VO}(\text{dha})(8\text{-hq})(\text{H}_2\text{O})]$ (1).

Bond Connectivity	Bond Length (Å)	Bond Connectivity	Dihedral Angle ($^\circ$)
$\text{O}(1)-\text{V}(13)$	1.9939	$\text{C}(2)-\text{O}(1)-\text{V}(13)-\text{O}(11)$	34.3999
$\text{O}(11)-\text{V}(13)$	2.1703	$\text{C}(2)-\text{O}(1)-\text{V}(13)-\text{O}(14)$	-166.2555
$\text{V}(13)-\text{O}(14)$	1.6047	$\text{C}(2)-\text{O}(1)-\text{V}(13)-\text{O}(25)$	-56.198
$\text{V}(13)-\text{N}(15)$	2.1108	$\text{C}(2)-\text{O}(1)-\text{V}(13)-\text{O}(26)$	105.4062
$\text{V}(13)-\text{O}(25)$	1.9261	$\text{C}(6)-\text{O}(11)-\text{V}(13)-\text{O}(1)$	-34.811
$\text{V}(13)-\text{O}(26)$	2.1528	$\text{C}(6)-\text{O}(11)-\text{V}(13)-\text{N}(15)$	134.0484
Bond Connectivity	Bond Angle ($^\circ$)	$\text{C}(6)-\text{O}(11)-\text{V}(13)-\text{O}(25)$	53.4449
$\text{O}(1)-\text{V}(13)-\text{O}(11)$	79.0591	$\text{C}(6)-\text{O}(11)-\text{V}(13)-\text{O}(26)$	-132.1167
$\text{O}(1)-\text{V}(13)-\text{O}(14)$	100.9314	$\text{O}(11)-\text{V}(13)-\text{N}(15)-\text{C}(16)$	88.6469
$\text{O}(1)-\text{V}(13)-\text{O}(25)$	88.3392	$\text{O}(11)-\text{V}(13)-\text{N}(15)-\text{C}(24)$	-92.5601
$\text{O}(1)-\text{V}(13)-\text{O}(26)$	93.4652	$\text{O}(14)-\text{V}(13)-\text{N}(15)-\text{C}(16)$	-71.1286
$\text{O}(11)-\text{V}(13)-\text{N}(15)$	84.5678	$\text{O}(14)-\text{V}(13)-\text{N}(15)-\text{C}(24)$	107.6643
$\text{O}(11)-\text{V}(13)-\text{O}(25)$	90.2716	$\text{O}(25)-\text{V}(13)-\text{N}(15)-\text{C}(16)$	179.8184
$\text{O}(11)-\text{V}(13)-\text{O}(26)$	72.0918	$\text{O}(25)-\text{V}(13)-\text{N}(15)-\text{C}(24)$	-1.3886
$\text{O}(14)-\text{V}(13)-\text{N}(15)$	98.2726	$\text{O}(26)-\text{V}(13)-\text{N}(15)-\text{C}(16)$	16.846
$\text{O}(14)-\text{V}(13)-\text{O}(25)$	110.0045	$\text{O}(26)-\text{V}(13)-\text{N}(15)-\text{C}(24)$	-164.361
$\text{O}(14)-\text{V}(13)-\text{O}(26)$	87.7144	$\text{O}(1)-\text{V}(13)-\text{O}(25)-\text{C}(23)$	165.0364
$\text{N}(15)-\text{V}(13)-\text{O}(25)$	80.6722	$\text{O}(11)-\text{V}(13)-\text{O}(25)-\text{C}(23)$	85.9902
$\text{N}(15)-\text{V}(13)-\text{O}(26)$	91.9625	$\text{O}(14)-\text{V}(13)-\text{O}(25)-\text{C}(23)$	-93.9326
$\text{V}(13)-\text{N}(15)-\text{C}(16)$	129.4489	$\text{N}(15)-\text{V}(13)-\text{O}(25)-\text{C}(23)$	1.5403
$\text{V}(13)-\text{N}(15)-\text{C}(24)$	110.7909	$\text{O}(1)-\text{V}(13)-\text{O}(26)-\text{H}(40)$	-63.8588
$\text{V}(13)-\text{O}(25)-\text{C}(23)$	117.3305	$\text{O}(1)-\text{V}(13)-\text{O}(26)-\text{H}(41)$	70.7578
$\text{V}(13)-\text{O}(26)-\text{H}(40)$	109.9603	$\text{O}(11)-\text{V}(13)-\text{O}(26)-\text{H}(40)$	13.4678
$\text{V}(13)-\text{O}(26)-\text{H}(41)$	117.8722	$\text{O}(11)-\text{V}(13)-\text{O}(26)-\text{H}(41)$	148.0844
$\text{C}(6)-\text{O}(11)-\text{V}(13)$	127.3622	$\text{O}(14)-\text{V}(13)-\text{O}(26)-\text{H}(40)$	-164.6783
$\text{C}(2)-\text{O}(1)-\text{V}(13)$	135.5302	$\text{O}(14)-\text{V}(13)-\text{O}(26)-\text{H}(41)$	-30.0617
		$\text{N}(15)-\text{V}(13)-\text{O}(26)-\text{H}(40)$	97.1167
		$\text{N}(15)-\text{V}(13)-\text{O}(26)-\text{H}(41)$	-128.2667
		$\text{V}(13)-\text{N}(15)-\text{C}(16)-\text{C}(17)$	178.5691
		$\text{V}(13)-\text{N}(15)-\text{C}(16)-\text{H}(34)$	-1.3695
		$\text{V}(13)-\text{N}(15)-\text{C}(24)-\text{C}(19)$	-178.8845
		$\text{V}(13)-\text{N}(15)-\text{C}(24)-\text{C}(23)$	1.0511
		$\text{V}(13)-\text{O}(1)-\text{C}(2)-\text{C}(3)$	-21.4677
		$\text{V}(13)-\text{O}(1)-\text{C}(2)-\text{C}(12)$	159.8808
		$\text{C}(3)-\text{C}(6)-\text{O}(11)-\text{V}(13)$	25.5657
		$\text{C}(7)-\text{C}(6)-\text{O}(11)-\text{V}(13)$	-155.7957
		$\text{C}(22)-\text{C}(23)-\text{O}(25)-\text{V}(13)$	178.7541
		$\text{C}(24)-\text{C}(23)-\text{O}(25)-\text{V}(13)$	-1.4277

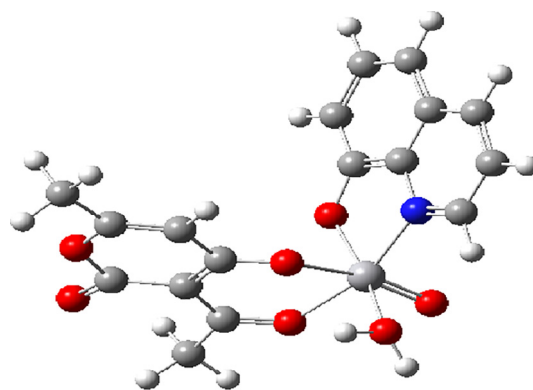


Fig. 6. Optimized molecular structure of the complex $\text{cis-}[\text{VO}(\text{dha})(8\text{-hq})(\text{H}_2\text{O})]$ (1).

the above geometrical data a suitable cis-octahedral geometry of the complex is suggested.

4.2. DFT-based molecular orbital analysis

Frontier molecular orbitals are significant to speculate and characterize the molecular chemical stability (Sun et al., 2003). Six important molecular orbitals (MOs) namely, HOMO, LUMO, two orbitals down to HOMO and two orbitals above the LUMO

were evaluated out for dehydroacetic acid (dhaH) and the complex. The analysis can be seen in Fig. S4(a) and (b). The electronic configuration can be used to verify diamagnetic nature of dhaH and paramagnetic behaviour of complex. From the overall composition the weakest bond is with H₂O reflected from bond length data as well as from orbital composition. The results are in good agreement as per the other existing scientific reports (Micera and Garribba, 2010). The HOMO-LUMO gap can be further co-related with ioniza-

tion energy (IE) and electron affinity (IA) by applying Koopmans's theorem (Mir et al., 2018). Above all, the global reactive descriptors can also be invoked as suggested elsewhere. The absolute electronegativity (χ_{abs}), absolute hardness (η) of dehydroacetic acid and its complex are represented in Table 2. Other important properties related to the dipole moment and hardness is electrophilicity index (ω), global softness (S) are given in Table 2.

Table 2

Absolute electronegativity (χ_{abs}), absolute hardness (η), electrophilicity index (ω), global softness (S) of complex [VO(dha)(8-hq)(H₂O)] (1).

Compounds	χ_{abs} (eV)	η (eV)	ω (Debye/eV)	S (eV)
Dehydroacetic acid	-4.907	-2.275	-1.237	-0.439
[VO(dha)(8-hq)(H ₂ O)]	-4.04765	-1.70633	-25.1725	-0.586054

Table 3

Calculated all Dipole moment (μ) components, Polarizability (α) and Hyperpolarizability (β) of complex [VO(dha)(8-hq)(H₂O)] (1).

Dipole moment (μ)		Hyperpolarizability(β)	
μ_x	-0.0509	β_{xxx}	233.0822
μ_y	9.1756	β_{yyy}	39.1697
μ_z	1.3079	β_{zzz}	21.4380
μ_{total}	9.2685	β_{xyy}	-45.0350
Polarizability(α)		β_{xxy}	87.5603
α_{xx}	-156.1946	β_{xxz}	-35.3639
α_{yy}	-143.0321	β_{xzz}	-45.3278
α_{zz}	-158.5821	β_{yzz}	8.9730
α_{xy}	-0.3631	β_{yyz}	1.0475
α_{xz}	-2.8886	β_{xyz}	36.9313
α_{yz}	8.1601	β_0	197.3575
α	-46.8815		
$\Delta\alpha$	14.5044		

Where, α_{xx} , α_{yy} and α_{zz} are tensor components of polarizability; β_{iiz} , β_{izi} and β_{zii} (i from x to z) are tensor components of hyperpolarizability; μ_x , μ_y and μ_z are the components of the dipole moment. α is the mean polarizability, $\Delta\alpha$ is the anisotropy of polarizability, β_0 is the mean first hyperpolarizability.

Table 4

Representation data of Mulliken and NBO atomic charges of complex [VO(dha)(8-hq)(H₂O)] (1).

S. No.	Atoms	NPA Atomic Charges	Mulliken Atomic Charges	S. No.	Atoms	NPA Atomic Charges	Mulliken Atomic Charges
1	O	-0.57638	-0.368434	29	H	0.24772	0.236485
2	C	0.59996	0.331365	30	H	0.23148	0.228213
3	C	-0.35975	-0.130355	31	H	0.24128	0.23666
4	C	0.79329	0.139277	32	H	0.25004	0.279743
5	O	-0.59679	-0.248496	33	H	0.26414	0.246581
6	C	0.50689	0.359207	34	H	0.22716	0.190448
7	C	-0.36453	-0.437214	35	H	0.23145	0.227117
8	C	0.44252	0.364391	36	H	0.2271	0.245285
9	C	-0.6718	-0.71309	37	H	0.21914	0.231091
10	O	-0.56866	-0.293461	38	H	0.22401	0.217495
11	O	-0.67835	-0.416197	39	H	0.23472	0.249412
12	C	-0.69091	-0.728677	40	H	0.54231	0.405731
13	V	0.79846	0.822877	41	H	0.53963	0.431262
14	O	-0.34507	-0.320039				
15	N	-0.45075	-0.300987				
16	C	0.11258	-0.21429				
17	C	-0.25248	-0.190082				
18	C	-0.13967	-0.320292				
19	C	-0.07139	0.462069				
20	C	-0.2411	-0.44823				
21	C	-0.18244	-0.163512				
22	C	-0.25486	-0.38737				
23	C	0.36853	0.332394				
24	C	0.16358	0.059503				
25	O	-0.626	-0.468221				
26	O	-0.88857	-0.667041				
27	H	0.24415	0.269074				
28	H	0.24933	0.250306				

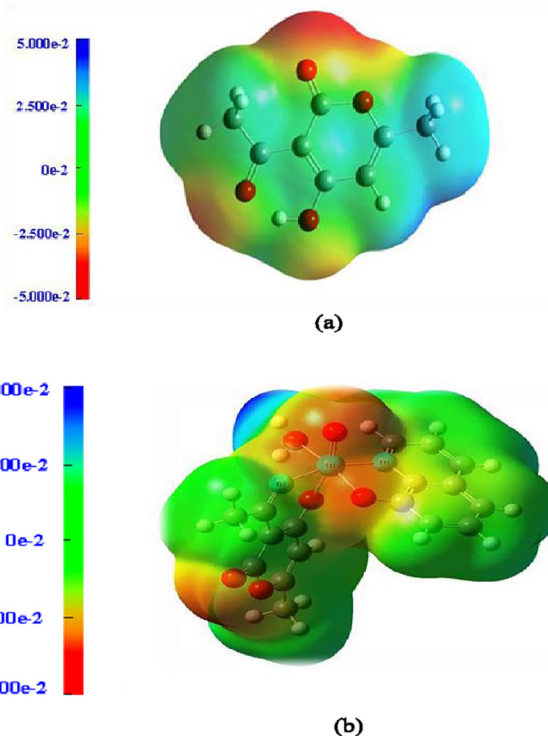


Fig. 7. Molecular electrostatic potential diagram of (a) dehydroacetic acid and (b) [VO(dha)(8-hq)(H₂O)] with color range along with scale.

4.3. Hyperpolarizability calculations

Density functional theory by the calculation of the dipole moment (μ), mean polarizability (α) and the total first static hyperpolarizability (β) is useful in predicting material properties of a compound (Manzoor et al., 2016; Islam and Pandith, 2014). The related information is helpful in gaining insights for the possible use in electronic, laser and photoactive devices. The respective data of [VO(dha)(8-hq)(H₂O)] in terms of x, y, z components are given in Table 3. It is here to mention that for the calculated electric dipole moment μ in Debye, isotropic polarizability α in a.u., anisotropy of the polarizability $\Delta\alpha$ in a.u., all hyperpolarizability (β) components in a.u. are the expressed units presented over here.

4.4. Molecular atomic charges and molecular electrostatic potential (MESP)

NBO and Mulliken population analysis of charges are the two hypothetical ways to explain the related partial charges of constituent atoms of a molecule. In case of the representative complex, [VO(dha)(8-hq)(H₂O)] the results shown by NBO and

Mulliken population analysis (Mulliken, 1995) under B3LYP/LANL2DZ basis set are shown in Table 4. The comparison between the two methods can be easily made by looking at the results. From the data the atoms namely C₂, C₄, C₆, C₈, C₂₃, C₂₄, V₁₃ and all hydrogen bear positive charge both in NBO and Mulliken analyses. The remaining atoms are negatively charged in both the analysis. The overall charge distribution is clearer from Fig. S5. It may be mentioned here that the natural population analysis is always made keeping in view the Pauli's exclusion principle (Mir et al., 2017a,b).

The molecular electrostatic potential surface of dehydroacetic acid and its vanadium complex are given in Fig. 7 (a) and (b), respectively. As expected, the diagram again predicts the predominance of charged regions within a molecular system. The MESP shows dehydroacetic acid having the carbonyl oxygen and hydroxyl oxygen atoms the most negative potential region, while in the case of the complex the coordination environment of four oxygen, one nitrogen and vanadium (central atom) is the region of most negative potential. The green region in the MESP surfaces represents neutral site between two extremes red and dark blue color or negative and positive charged loci. Table 5

Table 5
ESR spectral parameters of the complex, [VO(dha)(8-hq)(H₂O)] (1).

Compound	A _⊥	A	A _{av}	g _⊥	g	g _{av}
(1)	89	185	121	2.0301	2.0806	2.046

Table 6
Antibacterial study of the dha and the metal complex.

S. No.	Compound	Compound Zone of inhibition in (mm)			
		E. coli		S. pyogenes	
		Std.	E. coli	Std.	S. pyogenes
(1)	(dhaH)	33 ± 1.70	15 ± 2	12 ± 2	11 ± 2
(2)	[VO(dha)(8-hq)(H ₂ O)]	34 ± 1.50	14 ± 0.97	12 ± 1.50	13 ± 2

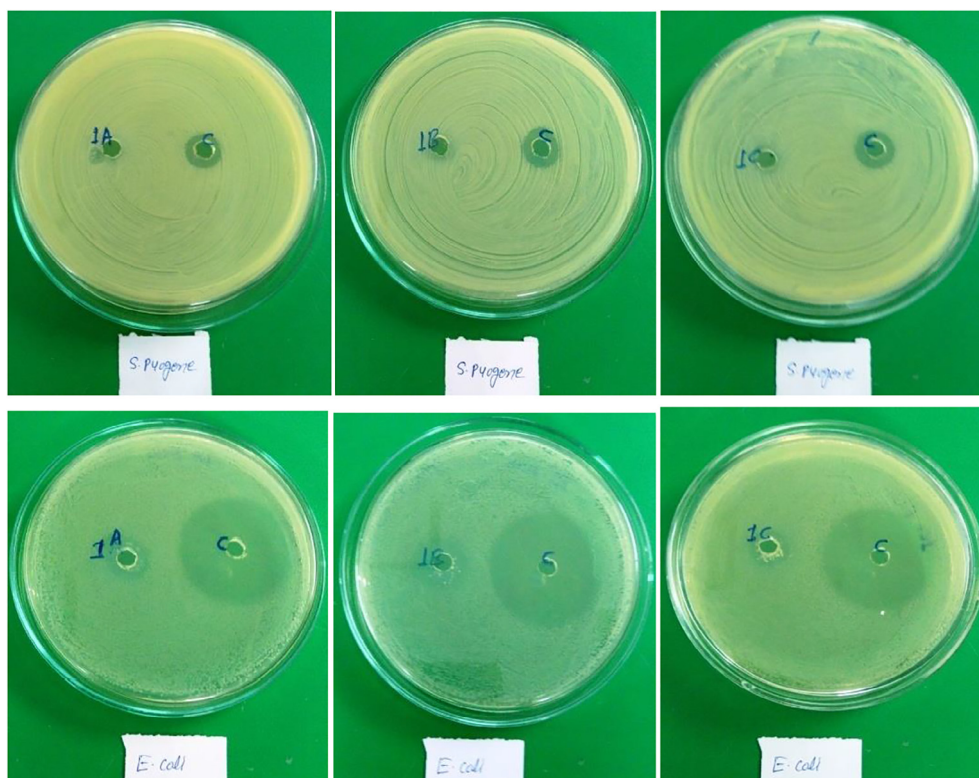


Fig. 8. Antibacterial activity of dhaH(1) and the complex against *S. pyogenes* and *E. coli*.

5. Antibacterial screening

The ligand and the metal complex were screened for their antibacterial activity against *E.coli* (MTCC16799), *S. pyogenes* (MTCC1925) at a concentration of 300- $\mu\text{g cm}^{-3}$ in DMSO by the agar well diffusion method. In the present same methodology was applied as reported elsewhere (Ong et al., 1994). Streptomycin was used as the standard antibacterial agent. All the experiments were carried out in triplicates. The results obtained in the study are the average readings of the data and have been presented in Table 6. From the measurement of inhibition zones indicated in Fig. 8, it is clear that the complex is less active against *E. coli*, but shows considerable activity against *S. pyogenes*, when compared with the standard drug. The activity index (AI) which is the ratio between inhibition zone of a sample to the inhibition zone of a standard drug can be used to explain the biological activity comparison between the subject compounds. From the results it is clear that AI value of the target complex against *S. pyogenes* is near about 1 and against *E. coli* it is very low than 1.

Both the activeness and passiveness against microbes can be thought useful in designing metal-relevant bio-remedial. It is essential to understand the microbial diversity in metal-rich environments and their metabolic capabilities to design effective bioremediation strategies. Systems biology approaches would aid in this direction. Systems biology is an integrative approach to study biological systems at the molecular, cellular, community, and ecosystem levels through interactions and networks. Knowledge on metal resistance gained through interdisciplinary approaches would aid in the design of effective metal bioremediation strategies.

6. Conclusions

The analytical data coupled with the studies presented above suggest that the oxovanadium(IV) complex in the present investigation is of the composition $[\text{VO}(\text{dha})(\text{L})(\text{H}_2\text{O})]$ were, dha = dehydroacetic acid, LH = 8-hydroxyquinolene. By the approach of different analytical techniques a cis-octahedral structure has been suggested for the complex. From the TG curve a good level of thermal resistance is evident. The satisfactory biological activity has been remarked against *S. Pyogenes* than *E. coli* as compared to the standard drugs. DFT-experimental results remained parallel to each other throughout the study except electronic spectral data wherein the agreement remained only around 400 nm region.

Acknowledgements

The author thankfully acknowledges Prof. Kapil Deo Mishra, Vice Chancellor, R. D. University Jabalpur, India, for his support in

developing the lab infrastructure. SAIF, IIT Mumbai, UGC networking Centre Hyderabad Central University and IIT, Chennai are also gratefully acknowledged for rendering necessary lab facilities.

Appendix A. Supplementary data

Supplementary data associated with this article can be found, in the online version, at <https://doi.org/10.1016/j.jksus.2018.03.023>.

References

- Dai, J. et al., 1996. *Polyhedron* 15, 1806.
- Diaz, C. et al., 2015. *J. Nanomater.* <https://doi.org/10.1155/2015/105157>.
- Dodd, J.W. et al., 1987. *Thermal Methods: Analytical Chemistry by Open Learning*. Wiley, New York, p. 73.
- Dutta, R.L., Syamal, A., 1993. *Electron Spin Resonance. In: Elements of Magnetochemistry*. 2nd ed. Affiliated East-West Press Pvt. Ltd, New Delhi, p. 225.
- Frisch M.J. et al., 2010. GAUSSIAN 09 (Revision C.01), Gaussian, Inc., Wallingford CT.
- Früh, N. et al., 2014. *Angew. Chem. Int. Ed.* 53, 10813.
- GaussView 5.0, Gaussian Inc., Carnegie office. Park. Pittsburgh. PA, USA.
- Greenwood, N.N., Earnshaw, A., 1984. *Chemistry of the Elements*. Pergamon Press, New York.
- Islam, N., Pandith, A.H., 2014. *J. Mol. Model.* 20, 2535.
- Jilal A.E. et al., 2017. *J. Mar. Chim. Heterocycl.* 16, N° 1
- Kumar, S. et al., 2009. *Mini-Rev. Med. Chem.* 9, 1648.
- Liu, Y. et al., 2014. *J. Diabetes Complicat.* 28, 265.
- Malik, B.A., Mir, J.M., 2018. *J. Coord. Chem.* <https://doi.org/10.1080/00958972.2018.1429600>.
- Mandewal, M.C. et al., 2016. *J. Saudi Chem. Soc.* 22, 218.
- Manzoor, T. et al., 2016. *Int. J. Quantum Chemi.* <https://doi.org/10.1002/qua.25332>.
- Maurya, R.C., Rajput, S., 2004. *J. Mol. Struct.* 35, 687.
- Maurya et al., 2015. *J. Coord. Chem.* 68 (16), 2902–2922.
- Maurya, R.C. et al., 2014. *J. Coord. Chem.* 67, 18.
- Maurya, R.C. et al., 2015. *J. Mole. Struct.* 1083, 343.
- Maurya, R.C. et al., 2001. *Indian J. Chem.* 40 (A), 1053.
- Maurya, R.C. et al., 2002. *Synth. React. Inorg.-Met. Org. Chem.* 32, 231–246.
- Micera, G., Garribba, E., 2010. *Eur. J. Inorg. Chem.* 4697. <https://doi.org/10.1002/ejic.201000382>.
- Micera, G., Garribba, E., 2011a. *Eur. J. Inorg. Chem.* 3768. <https://doi.org/10.1002/ejic.201100422>.
- Micera, G., Garribba, E., 2011b. *J. Comp. Chem.* 32, 2822.
- Mir et al., 2018. *J. Chinese Adv. Mater. Soc.* 6, 55.
- Mir, J.M. et al., 2017. *Nov. Appro. Drug Des. Dev.* 1 (5). NAPDD.MS.ID.555574.
- Mir, J.M. et al., 2017. *Karbala Int. J. Modern Sci.* 3, 212.
- Mir, M.J. et al., 2016. *J. Theor. Comput. Sci.* 3. <https://doi.org/10.4172/2376-130X.1000147>.
- Ong, E.O. et al., 1994. *I. L Farmaco* 49, 513.
- Popova, T.V. et al., 2015. *Russian Chemical Bulletin. International Edition* 64, 1857.
- Rodrigues, G.S., 2011. *Inc. Int. J. Quant. Chem.* 111, 1395.
- Sasmal, P.K. et al., 2008. *J. Inorg. Biochem.* 102, 1463.
- Singh, H. et al., 2013. *Biointerface Res. Appl. Chem.* 3, 484.
- Sun, Y. et al., 2003. *J. Chem. Phys. Lett.* 381, 397.
- Thompson, K.H., Orvig, C., 2006. *J. Inorg. Biochem.* 100, 1925.
- Valenzuela, C.D. et al., 2013. *Sci. Rep.* 3, 2642.
- Vishwakarma, P.K. et al., 2016. *J. Chem. Sci.* 128, 511.